Spectral Measurement of Electron Antineutrino Oscillation Amplitude and Frequency at Daya Bay

F. P. An,[1,2] A. B. Balantekin,[3] H. R. Band,[3] W. Beriguete,[4] M. Bishai,[4] S. Blyth,[5] R. L. Brown,[4] I. Butorov,[6] G. F. Cao,[1] J. Cao,[1] R. Carr,[7] Y. L. Chan,[8] J. F. Chang,[1] Y. Chang,[9] C. Chasman,[4] H. S. Chen,[1] H. Y. Chen,[10] S. J. Chen,[11] S. M. Chen,[12] X. C. Chen,[8] X. H. Chen,[1] Y. Chen,[13] Y. X. Chen,[14] Y. P. Cheng,[1] J. J. Cherwinka,[3] M. C. Chu,[8] J. P. Cummings,[15] J. de Arcos,[16] Z. Y. Deng,[1] Y. Y. Ding,[1] M. V. Diwan,[4] E. Draeger,[16] X. F. Du,[1] D. A. Dwyer,[17] W. R. Edwards,[17,18] S. R. Ely,[19] J. Y. Fu,[1] L. Q. Ge,[20] R. Gill,[4] M. Gonchar,[6] G. H. Gong,[12] H. Gong,[12] Y. A. Gornushkin,[6] W. Q. Gu,[21] M. Y. Guan,[1] X. H. Guo,[22] R. W. Hackenburg,[4] R. L. Hahn,[4] G. H. Han,[23] S. Hans,[4] M. He,[1] K. M. Heeger,[24] Y. K. Heng,[1] P. Hinrichs,[3] yk. Hor,[25] Y. B. Hsiung,[5] B. Z. Hu,[10] L. J. Hu,[22] L. M. Hu,[4] T. Hu,[1] W. Hu,[1] E. C. Huang,[19] H. X. Huang,[26] H. Z. Huang,[27] X. T. Huang,[28] P. Huber,[25] G. Hussain,[12] Z. Isvan,[4] D. E. Jaffe,[4] P. Jaffke,[25] S. Jetter,[1] X. L. Ji,[1] X. P. Ji,[29] H. J. Jiang,[20] J. B. Jiao,[28] R. A. Johnson,[30] L. Kang,[31] S. H. Kettell,[4] M. Kramer,[17,18] K. K. Kwan,[8] M. W. Kwok,[8] T. Kwok,[32] W. C. Lai,[20] W. H. Lai,[10] K. Lau,[33] L. Lebanowski,[12] J. Lee,[17] R. T. Lei,[31] R. Leitner,[34] A. Leung,[32] J. K. C. Leung,[32] C. A. Lewis,[3] D. J. Li,[35] F. Li,[1] G. S. Li,[21] Q. J. Li,[1] W. D. Li,[1] X. N. Li,[1] X. Q. Li,[29] Y. F. Li,[1] Z. B. Li,[36] H. Liang,[35] C. J. Lin,[17] G. L. Lin,[10] S. K. Lin,[33] Y. C. Lin,[20] J. J. Ling,[4] J. M. Link,[25] L. Littenberg,[4] B. R. Littlejohn,[30] D. W. Liu,[19,33] H. Liu,[33] J. C. Liu,[1] J. L. Liu,[21] S. S. Liu,[32] Y. B. Liu,[1] C. Lu,[37] H. Q. Lu,[1] K. B. Luk,[17,18] Q. M. Ma,[1] X. B. Ma,[14] X. Y. Ma,[1] Y. Q. Ma,[1] K. T. McDonald,[37] M. C. McFarlane,[3] R. D. McKeown,[23] Y. Meng,[25] I. Mitchell,[33] Y. Nakajima,[17] J. Napolitano,[38] D. Naumov,[6] E. Naumova,[6] I. Nemchenok,[6] H. Y. Ngai,[32] W. K. Ngai,[19] Z. Ning,[1] J. P. Ochoa-Ricoux,[17] A. Olshevski,[6] S. Patton,[17] V. Pec,[34] J. C. Peng,[19] L. E. Piilonen,[25] L. Pinsky,[33] C. S. J. Pun,[32] F. Z. Qi,[1] M. Qi,[11] X. Qian,[4,7] N. Raper,[38] B. Ren,[31] J. Ren,[26] R. Rosero,[4] B. Roskovec,[34] X. C. Ruan,[26] B. B. Shao,[12] H. Steiner,[17,18] G. X. Sun,[1] J. L. Sun,[39] Y. H. Tam,[8] H. K. Tanaka,[4] X. Tang,[1] H. Themann,[4] S. Trentalange,[27] O. Tsai,[27] K. V. Tsang,[17] R. H. M. Tsang,[7] C. E. Tull,[17] Y. C. Tung,[5] B. Viren,[4] V. Vorobel,[34] C. H. Wang,[9] L. S. Wang,[1] L. Y. Wang,[1] L. Z. Wang,[14] M. Wang,[28] N. Y. Wang,[22] R. G. Wang,[1] W. Wang,[23] W. W. Wang,[11] X. Wang,[40] Y. F. Wang,[1] Z. Wang,[12] Z. Wang,[1] Z. M. Wang,[1] D. M. Webber,[3] H. Wei,[12] Y. D. Wei,[31] L. J. Wen,[1] K. Whisnant,[41] C. G. White,[16] L. Whitehead,[33] T. Wise,[3] H. L. H. Wong,[17,18] S. C. F. Wong,[8] E. Worcester,[4] Q. Wu,[28] D. M. Xia,[1] J. K. Xia,[1] X. Xia,[28] Z. Z. Xing,[1] J. Xu,[22] J. L. Xu,[1] J. Y. Xu,[8] Y. Xu,[29] T. Xue,[12] J. Yan,[42] C. G. Yang,[1] L. Yang,[31] M. S. Yang,[1] M. Ye,[1] M. Yeh,[4] Y. S. Yeh,[10] B. L. Young,[41] G. Y. Yu,[11] J. Y. Yu,[12] Z. Y. Yu,[1] S. L. Zang,[11] L. Zhan,[1] C. Zhang,[4] F. H. Zhang,[1] J. W. Zhang,[1] Q. M. Zhang,[42] S. H. Zhang,[1] Y. C. Zhang,[35] Y. H. Zhang,[1] Y. M. Zhang,[12] Y. X. Zhang,[39] Z. J. Zhang,[31] Z. P. Zhang,[35] Z. Y. Zhang,[1] J. Zhao,[1] Q. W. Zhao,[1] Y. B. Zhao,[1] L. Zheng,[35] W. L. Zhong,[1] L. Zhou,[1] Z. Y. Zhou,[26] H. L. Zhuang[1] and J. H. Zou[1]

(Daya Bay Collaboration)

[1]*Institute of High Energy Physics, Beijing*
[2]*East China University of Science and Technology, Shanghai*
[3]*University of Wisconsin, Madison, Wisconsin*
[4]*Brookhaven National Laboratory, Upton, New York*
[5]*Department of Physics, National Taiwan University, Taipei*
[6]*Joint Institute for Nuclear Research, Dubna, Moscow Region*
[7]*California Institute of Technology, Pasadena, California*
[8]*Chinese University of Hong Kong, Hong Kong*
[9]*National United University, Miao-Li*
[10]*Institute of Physics, National Chiao-Tung University, Hsinchu*
[11]*Nanjing University, Nanjing*
[12]*Department of Engineering Physics, Tsinghua University, Beijing*
[13]*Shenzhen Univeristy, Shenzhen*
[14]*North China Electric Power University, Beijing*
[15]*Siena College, Loudonville, New York*
[16]*Department of Physics, Illinois Institute of Technology, Chicago, Illinois*
[17]*Lawrence Berkeley National Laboratory, Berkeley, California*
[18]*Department of Physics, University of California, Berkeley, California*
[19]*Department of Physics, University of Illinois at Urbana-Champaign, Urbana, Illinois*
[20]*Chengdu University of Technology, Chengdu*
[21]*Shanghai Jiao Tong University, Shanghai*

[22]Beijing Normal University, Beijing
[23]College of William and Mary, Williamsburg, Virginia
[24]Department of Physics, Yale University, New Haven, Connecticut
[25]Center for Neutrino Physics, Virginia Tech, Blacksburg, Virginia
[26]China Institute of Atomic Energy, Beijing
[27]University of California, Los Angeles, California
[28]Shandong University, Jinan
[29]School of Physics, Nankai University, Tianjin
[30]Department of Physics, University of Cincinnati, Cincinnati, Ohio
[31]Dongguan University of Technology, Dongguan
[32]Department of Physics, The University of Hong Kong, Pokfulam, Hong Kong
[33]Department of Physics, University of Houston, Houston, Texas
[34]Charles University, Faculty of Mathematics and Physics, Prague
[35]University of Science and Technology of China, Hefei
[36]Sun Yat-Sen (Zhongshan) University, Guangzhou
[37]Joseph Henry Laboratories, Princeton University, Princeton, New Jersey
[38]Department of Physics, Applied Physics, and Astronomy, Rensselaer Polytechnic Institute, Troy, New York
[39]China Guangdong Nuclear Power Group, Shenzhen
[40]College of Electronic Science and Engineering, National University of Defense Technology, Changsha
[41]Iowa State University, Ames, Iowa
[42]Xi'an Jiaotong University, Xi'an

(Received 24 October 2013; published 10 February 2014)

A measurement of the energy dependence of antineutrino disappearance at the Daya Bay reactor neutrino experiment is reported. Electron antineutrinos ($\bar{\nu}_e$) from six 2.9 GW_{th} reactors were detected with six detectors deployed in two near (effective baselines 512 and 561 m) and one far (1579 m) underground experimental halls. Using 217 days of data, 41 589 (203 809 and 92 912) antineutrino candidates were detected in the far hall (near halls). An improved measurement of the oscillation amplitude $\sin^2 2\theta_{13} = 0.090^{+0.008}_{-0.009}$ and the first direct measurement of the $\bar{\nu}_e$ mass-squared difference $|\Delta m^2_{ee}| = (2.59^{+0.19}_{-0.20}) \times 10^{-3}$ eV^2 is obtained using the observed $\bar{\nu}_e$ rates and energy spectra in a three-neutrino framework. This value of $|\Delta m^2_{ee}|$ is consistent with $|\Delta m^2_{\mu\mu}|$ measured by muon neutrino disappearance, supporting the three-flavor oscillation model.

DOI: 10.1103/PhysRevLett.112.061801 PACS numbers: 14.60.Pq, 13.15.+g, 28.50.Hw, 29.40.Mc

Experimental measurements of neutrino oscillations have clearly established that neutrinos have mass and that the mass eigenstates mix [1]. The Daya Bay experiment recently reported the discovery of the disappearance of reactor antineutrinos over kilometer-long baselines, providing the most precise measurement of the mixing angle θ_{13} [2,3]. Other experiments have made consistent θ_{13} measurements [4–7]. Precise knowledge of neutrino mixing and mass differences enables experimental searches for CP violation, tests of the neutrino mass hierarchy, and precision tests of oscillation theory. In particular, the relatively large value of θ_{13} facilitates a rich program of future neutrino oscillation research [8–10]. It also allows the Daya Bay experiment to report in this Letter an independent measurement of the neutrino mass splitting via the distortion of the reactor antineutrino energy spectrum.

In the framework of three-flavor neutrino mixing in vacuum, the probability that an $\bar{\nu}_e$ produced with energy E is detected as an $\bar{\nu}_e$ at a distance L is given by

$$P_{\bar{\nu}_e \to \bar{\nu}_e} = 1 - \cos^4\theta_{13}\sin^2 2\theta_{12}\sin^2\Delta_{21} - \sin^2 2\theta_{13}(\cos^2\theta_{12}\sin^2\Delta_{31} + \sin^2\theta_{12}\sin^2\Delta_{32}), \quad (1)$$

where $\Delta_{ji} \equiv 1.267\Delta m^2_{ji}(\mathrm{eV}^2)[L(\mathrm{m})/E(\mathrm{MeV})]$, and Δm^2_{ji} is the difference between the mass squares of the mass eigenstates ν_j and ν_i. Since $\Delta m^2_{21} \ll |\Delta m^2_{31}| \approx |\Delta m^2_{32}|$ [1], the short-distance (~km) reactor $\bar{\nu}_e$ oscillation is due primarily to the Δ_{3i} terms and naturally leads to the definition of the effective mass-squared difference $\sin^2\Delta_{ee} \equiv \cos^2\theta_{12}\sin^2\Delta_{31} + \sin^2\theta_{12}\sin^2\Delta_{32}$ [11].

The Daya Bay experiment previously determined $\sin^2 2\theta_{13}$ using only the relative rates of $\bar{\nu}_e$ detected in three antineutrino detectors (ADs) located near to and three ADs located far from six nuclear reactor cores [2,3]. The effective mass splitting $|\Delta m^2_{\mu\mu}|$ measured in ν_μ disappearance [12] provided a good approximation of $|\Delta m^2_{ee}|$ in the rate-only measurement. This Letter presents a combined analysis of the $\bar{\nu}_e$ rates and energy spectra measured for the six detector data-taking period from 24 December 2011 to 28 July 2012. This represents a 48% increase in statistics over the most recent result [3]. The $\sin^2 2\theta_{13}$ uncertainty is reduced by inclusion of the spectral information and the statistics of the complete six-AD data period. The spectral distortion due to the $\sin^2\Delta_{ee}$ term provides a strong confirmation that the observed $\bar{\nu}_e$ deficit is consistent with

neutrino oscillations and allows the first direct measurement of $|\Delta m^2_{ee}|$.

A detailed description of the Daya Bay experiment can be found in [13,14]. Each of the three experimental halls (EHs) contains functionally identical, three-zone ADs surrounded by a pool of ultrapure water segmented into two regions, the inner water shield (IWS) and outer water shield (OWS), which are instrumented with photomultiplier tubes (PMTs). In each AD, light created as a result of particle interactions in the innermost zone, defined by an inner acrylic vessel (IAV) containing gadolinium-doped liquid scintillator (LS), and the surrounding undoped LS zone, is collected by 192 radially positioned 20-cm PMTs in the outermost mineral-oil region. The AD trigger threshold of 45 hit PMTs or a summed charge of ~65 photoelectrons in all PMTs corresponds to about 0.4 MeV in the Gd-doped volume. The trigger inefficiency for events above 0.7 MeV is negligible. Charge and timing information for each PMT are available for energy calibration and reconstruction, as described in Ref. [13]. The detectors have a light yield of ~165 photoelectrons/MeV and a reconstructed energy resolution of $\sigma_E/E \approx 8\%$ at 1 MeV.

Reactor antineutrinos are detected via the inverse β-decay (IBD) reaction, $\bar{\nu}_e + p \to e^+ + n$. The delayed gamma rays (totaling ~8 MeV) generated from the neutron capture on Gd with a mean capture time of ~30 μs enable powerful background suppression. The prompt light from the e^+ gives an estimate of the incident $\bar{\nu}_e$ energy, $E_{\bar{\nu}_e} = E_{\text{prompt}} + \bar{E}_n + 0.78$ MeV, where E_{prompt} is the prompt event energy including the positron kinetic energy and the annihilation energy, and $\bar{E}_n$ is the average neutron recoil energy (~10 keV).

Interpretation of the observed prompt energy spectra requires characterization of the detector response to e^+, e^-, and γ, which maps the true energy (E_{true}) to the reconstructed energy (E_{rec}). E_{rec} is determined by scaling the measured total charge with a position-dependent correction [3,13]. For a γ or e^-, E_{true} is the kinetic energy; for a positron E_{true} is the sum of the kinetic energy and the energy from annihilation. The energy response is not linear due to scintillator and electronics effects and is taken into account by two functions, f_{scint} and f_{elec}, respectively. The scintillator nonlinearity is particle and energy dependent, and is related to intrinsic scintillator quenching and Cherenkov light emission. The quenching effects are constrained by standalone measurements with a fast neutron beam as well as by neutron source data and radioactive α decays in the AD. The Cherenkov contribution is also affected by absorption and reemission in the liquid scintillator. The scintillator nonlinearity for electrons is described by an empirical model $f_{\text{scint}}(E_{\text{true}}) = E_{\text{vis}}/E_{\text{true}} = (p_0 + p_3 E_{\text{true}})/(1 + p_1 e^{-p_2 E_{\text{true}}})$, where E_{vis} is the total visible light generated by the particle and p_i are the model parameters. A GEANT4-based [15,16] Monte Carlo simulation (MC) is used to relate the e^- scintillator nonlinearity to the response for γ and e^+. The electronics nonlinearity, $f_{\text{elec}}(E_{\text{vis}})$, is introduced due to the interaction of the scintillation light time profile and the charge collection of the front-end electronics. Given the similar timing profiles for $e^\pm$ and γs, it is modeled as an exponential function of E_{vis} as determined by studying the time profile of charge in the data and MC.

The energy model, $f = f_{\text{scint}} \times f_{\text{elec}}$, is determined by a fit to monoenergetic γ lines from radioactive sources and the continuous $\beta + \gamma$ spectrum extracted from ^{12}B data. Sources were deployed at the center of all ADs regularly (^{68}Ge, ^{60}Co, ^{241}Am-^{13}C) [13] and during a special calibration period in summer 2012 (^{137}Cs, ^{54}Mn, ^{40}K, ^{241}Am-^{9}Be, Pu-^{13}C) with AD1 and AD2 in the near-hall EH1. In addition, gamma peaks in all ADs which could be identified with singles and correlated spectra in data (^{40}K, ^{208}Tl, n capture on H, C, and Fe) were included. For source data with multiple gamma-line emissions, f_{scint} is computed for each gamma then summed up, whereas f_{elec} is computed based on the total E_{vis}. The ^{12}B isotopes are produced cosmogenically at the rate of about 900 (60) events/day/AD at the near (far) site. The measured relative nonlinearity of $< 0.3\%$ among 6 ADs [3] is negligible in the context of the energy model.

Figure 1 compares the best-fit energy model with the single-gamma, multigamma, and continuous ^{12}B data used to determine the model parameters. As additional validation, the energy model prediction for the continuous $\beta + \gamma$ spectra from ^{212}Bi, ^{214}Bi, and ^{208}Tl decays was compared with the data and found to be consistent.

Alternative energy response models, based on different methodologies, were constructed. The second method builds the scintillator nonlinearity based on Birks' formula [17] and Cherenkov radiation theory. The model is characterized by Birks' constant k_B and the Cherenkov light contribution k_c. f_{elec} is determined from the residual nonlinearity of the same γ and β-decay calibration data set. The third method does not use γ data but only uses β decay from ^{12}B, as well as the internal radioactive β decays of ^{212}Bi, ^{214}Bi, and ^{208}Tl, to construct the energy model.

All positron energy response models were consistent with each other to ~1.5%. The uncertainty in the e^+ energy response, shown in Fig. 1, is conservatively estimated by combining the calibration and model uncertainties. The energy response has a marginal effect on the measured oscillation parameters because it is essentially identical for all ADs.

The observed prompt energy spectrum is modified because positrons from IBD interactions near the IAV can deposit energy in the acrylic without generating scintillation light. This significantly affects ~1% of all IBD positrons causing an enhancement near $E_{\text{rec}} \approx 1$ MeV that is taken into account using MC.

The analysis used for previous Daya Bay results [2,3] has been repeated with the full six-AD data sample. The rate uncertainty of the background is slightly reduced

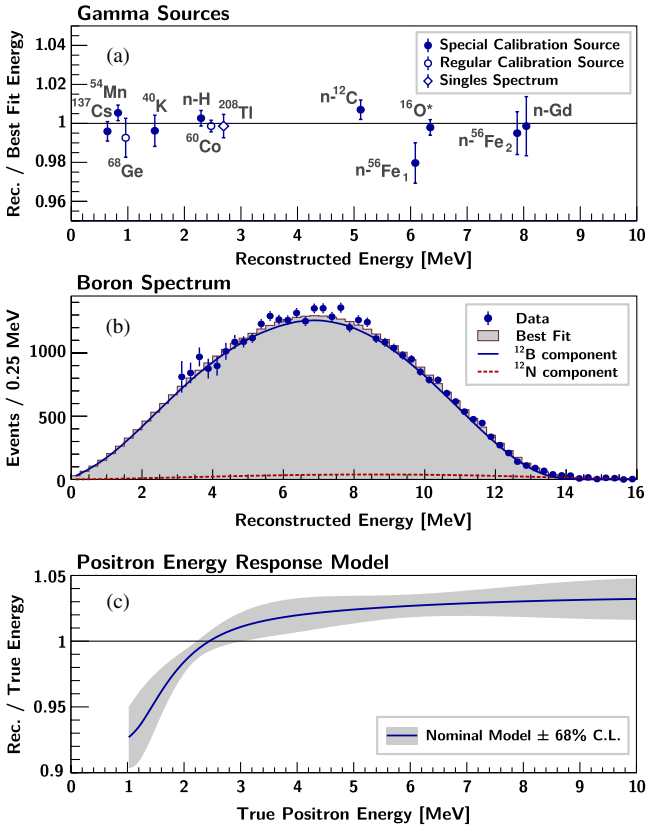

FIG. 1 (color online). (a) Ratio of the reconstructed to best-fit energies of γ lines from calibration sources and singles spectra as described in the text. The error bars represent the total uncertainty on each ratio. The γ from the second-excited state of ^{16}O in the Pu-^{13}C source is denoted $^{16}O^{*}$. The n-^{56}Fe$_1$ and n-^{56}Fe$_2$ labels denote the ~6 MeV and ~7.6 MeV γs, respectively, resulting from the capture of neutrons from the AmC sources parked on top of the AD. (b) Reconstructed energy spectrum (points) compared to the sum (shaded area) of the ^{12}B (solid line) and ^{12}N (dashed line) components of the best-fit energy response model. The error bars represent the statistical uncertainties. (c) AD energy response model for positrons.

compared to the previous analysis due to the increased statistics. The rate-only analysis yields $\sin^2 2\theta_{13} = 0.090 \pm 0.010$ with $\chi^2/\mathrm{NDF} = 0.6/4$, where NDF is the number of degrees of freedom. The analysis has also been updated to include spectral information by applying the energy nonlinearity correction to the positron spectrum and measuring the spectral distribution of the five background sources. The spectral uncertainties of the five backgrounds are included as uncorrelated among energy bins in the χ^2 fit of the oscillation parameters, to allow all possible spectral models consistent with the data. The combined rate and spectral analysis yields $\sin^2 2\theta_{13} = 0.092 \pm 0.008$ and $|\Delta m^2_{ee}| = (2.57^{+0.20}_{-0.22}) \times 10^{-3}\ \mathrm{eV}^2$ with $\chi^2/\mathrm{NDF} = 166/171$, which are consistent with the results to be described in this Letter.

This Letter presents the results of an analysis that is largely independent of the analysis described in [2,3]. The two analyses differ in terms of event reconstruction, energy calibration, IBD selection, background estimation, and construction of the χ^2 used for determination of the oscillation parameters. The selected IBD candidates differ by 3.7% (11%) at the far (near) sites. A "blind analysis" strategy was implemented by concealing the reactor history and thermal power information for all cores for the new data period.

IBD candidates are selected with the criteria that follows. First, events caused by PMT light emission are efficiently removed using the techniques of [3]. Candidates are then selected by requiring a promptlike signal (0.7–12 MeV) in coincidence with a delayedlike signal (6–12 MeV) separated by 1–200 μs. Candidate pairs are vetoed if their delayedlike events occur (i) within a (-2 μs, 600 μs) time window with respect to an IWS or OWS trigger with a PMT multiplicity > 12, (ii) within a (-2 μs, 1400 μs) time window with respect to triggers in the same AD with a total light yield larger than 3000 photoelectrons, or (iii) within a (-2 μs, 0.4 s) time window with respect to triggers in the same AD with a total light yield higher than 3×10^5 photoelectrons. This targeted muon veto allows for efficient removal of spurious triggers that follow a muon as well as most muon-induced spallation products. Finally, a multiplicity cut is applied to remove any ambiguities in the IBD pair selection. This cut requires no additional promptlike signals 400 μs before the delayed event, and no delayedlike signals 200 μs after the delayed event. The muon veto efficiency (ε_μ) and multiplicity cut efficiency (ε_m) are calculated directly from data with negligible uncertainties for each AD. The average values of $\varepsilon_\mu \cdot \varepsilon_m$ are summarized in Table I.

A detailed treatment of the absolute and relative efficiencies, as well as their corresponding uncertainties, has been reported in [3,13]. The uncertainties of the absolute efficiencies are correlated among ADs and thus play a negligible role in the extraction of the oscillation parameters. All differences among ADs are treated as uncorrelated uncertainties. In the rate-only analysis, the uncorrelated uncertainties are dominated by the delayed-energy cut (0.12%) and Gd capture fraction ($< 0.1\%$). In the spectral analysis, additional uncorrelated uncertainty comes from the relative energy scale difference between ADs. Based upon the relative response in all ADs to identified gamma and alpha peaks from numerous sources that span the IBD positron energy range, a 0.35% uncertainty is assigned.

Five sources of background are identified. The accidental background, defined as any pair of otherwise uncorrelated signals that happen to satisfy the IBD selection criteria, is the largest background in the antineutrino sample. The rate and energy spectra of this background can be accurately determined by measuring the singles rates of prompt- and delayedlike signals and then calculating the probability that the two randomly satisfy the selection criteria. Alternative estimation methods yield consistent results. The relative uncertainty of this background is 0.3% and is dominated by the statistics in the rate of delayedlike signals.

TABLE I. Summary of signal and backgrounds. The background and IBD rates are corrected for the product of the muon veto and multiplicity cut efficiencies $\varepsilon_\mu \cdot \varepsilon_m$.

	EH1		EH2		EH3	
	AD1	AD2	AD3	AD4	AD5	AD6
IBD candidates	101 290	102 519	92 912	13 964	13 894	13 731
Data acquisition live time (days)	191.001		189.645		189.779	
$\varepsilon_\mu \cdot \varepsilon_m$	0.7957	0.7927	0.8282	0.9577	0.9568	0.9566
Accidentals (per day)	9.54 ± 0.03	9.36 ± 0.03	7.44 ± 0.02	2.96 ± 0.01	2.92 ± 0.01	2.87 ± 0.01
Fast-neutron (per AD per day)	0.92 ± 0.46		0.62 ± 0.31		0.04 ± 0.02	
^{9}Li/^{8}He (per AD per day)	2.40 ± 0.86		1.20 ± 0.63		0.22 ± 0.06	
Am-C correlated (per AD per day)	0.26 ± 0.12					
^{13}C$(\alpha, n)^{16}$O background (per day)	0.08 ± 0.04	0.07 ± 0.04	0.05 ± 0.03	0.04 ± 0.02	0.04 ± 0.02	0.04 ± 0.02
IBD rate (per day)	653.30 ± 2.31	664.15 ± 2.33	581.97 ± 2.07	73.31 ± 0.66	73.03 ± 0.66	72.20 ± 0.66

The correlated $\beta - n$ decays from cosmogenic ^{9}Li and ^{8}He can mimic IBD interactions. The rate of correlated background from this source is estimated by fitting the distribution of the time elapsed since the last muon with the known ^{9}Li and ^{8}He decay lifetimes [18]. The 20% systematic uncertainty takes into account the uncertainty in ^{9}Li and ^{8}He production by muons with energy below the showering muon threshold. The rate is assumed to be the same for ADs at the same site. The fraction of ^{9}Li events in this background is estimated to be $95\% \pm 5\%$ based on data and MC. The spectra are calculated with a model that simulates the decay chain of each isotope into their daughters based on external data [19,20]. The spectral uncertainty of this background is estimated by assigning large variations to the energy response model, particularly for the neutron and alpha daughter particles.

Neutrons from the ~0.7 Hz Am-C calibration sources inside the automated calibration units on top of the ADs can occasionally mimic IBD events by inelastically scattering with nuclei in the shielding material and then capturing on Fe/Cr/Mn/Ni. This produces two γ rays that both enter the scintillating region. The MC is used to estimate the rate of this background. The normalization is constrained by the measured rate of single delayedlike candidates from this source. A special Am-C source, approximately 80 times more potent than the calibration sources, was temporarily deployed during summer 2012. Results from this source are used to benchmark the MC and provide the estimate of the 45% uncertainty in the rate normalization. The energy spectrum of this background is modeled as an exponential, the parameters of which are constrained by these data.

Through elastic scattering with protons and the subsequent thermalization and capture on gadolinium, energetic neutrons produced by cosmic rays can mimic IBD interactions. The energy of the proton-recoil signal ranges from sub-MeV up to several hundred MeV. If the prompt energy criterion is loosened to (0.7–50) MeV, a flat spectrum is observed up to 50 MeV, which is extrapolated into the IBD energy region. The flat spectrum assumption is corroborated through the study of fast neutrons associated with muons identified by the muon veto system and by MC. A 50% systematic uncertainty in the rate is assigned. The rate is assumed to be the same for ADs in the same experimental hall.

The ^{13}C$(\alpha, n)^{16}$O background is determined from a simulation adjusted with the measured alpha-decay rates from ^{238}U, ^{232}Th, ^{227}Ac, and ^{210}Po decay chains. This background represents only about 0.01% and 0.05% of the total IBD sample in the near and far sites, respectively.

The estimated IBD and background rates are summarized in Table I and displayed in Fig. 2. Backgrounds amount to about 5% (2%) of the IBD candidate sample in the far (near) sites.

The $\bar{\nu}_e$ spectrum from a reactor with thermal power $W_{\rm th}(t)$ at energy E and on a given day t is

$$\frac{d^2N(E,t)}{dEdt} = \sum_i \left(\frac{W_{\rm th}(t)}{\sum_j f_j(t) e_j} f_i(t) S_i(E) c_i^{\rm ne}(E,t) \right) + S_{\rm SNF}(E,t),$$

with the fission fractions from each isotope $f_i(t)$, the thermal energy released per fission for each isotope e_i, the $\bar{\nu}_e$ yield per fission for each isotope $S_i(E)$, the correction to the $\bar{\nu}_e$ yield due to reactor nonequilibrium effects $c_i^{\rm ne}(E,t)$ and the spent nuclear fuel $S_{\rm SNF}(E,t)$. The nuclear reactor operators provide daily effective livetime-corrected thermal power as well as periodic burn-up and simulation-based fission fraction data that are used to calculate daily fission fractions. The $\bar{\nu}_e$ flux at each detector is calculated by summing the contributions of all reactors. The treatment of $W_{\rm th}$, f_i, e_i, $c_i^{\rm ne}$, and $S_{\rm SNF}$ terms are described in [2,3]. The integrated, livetime-corrected, exposure for the EH3 ADs is 168.8 kton·GW$_{\rm th}$·day with mean fission fractions ^{235}U:^{238}U:^{239}Pu:^{241}Pu = 0.573:0.076:0.301:0.050. Because of the relative measurement of near and far detectors, the measurement of oscillation parameters is insensitive to the choice of $S_i(E)$ [21–26].

The oscillation parameters are extracted from a fit that takes into account the antineutrino rate, spectral

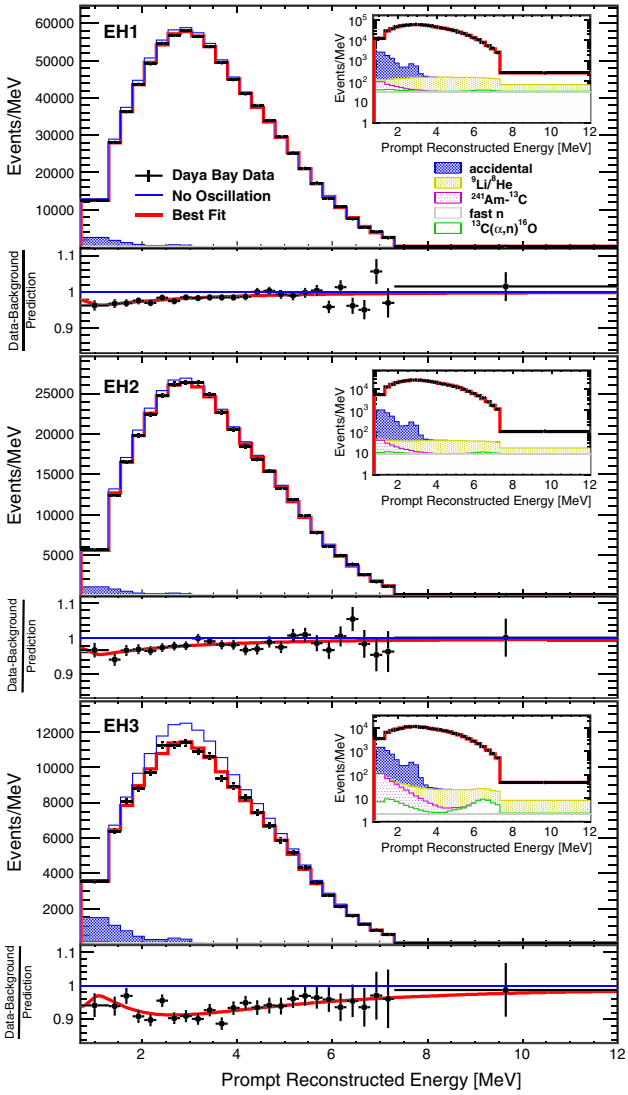

FIG. 2 (color online). The upper panel in each pair of panels shows the prompt positron spectra (black points) measured in the near (EH1 and EH2) and far (EH3) experimental halls with the best-fit background contribution (shaded and colored regions). The thick red (thin blue) histograms represent the expected best-fit (no-oscillations) spectra. The inset in each panel shows the same spectra with a logarithmic ordinate. In the lower panel in each pair, the black points represent the ratio of the background-subtracted data divided by the predicted no-oscillation spectra. The error bars represent the statistical uncertainty only. The red curve in each lower panel represents the ratio of the best-fit to no-oscillations spectra. The change in slope of the red curve in the lowest energy bin is due to the effect of energy loss in the acrylic.

information, and the $\bar{\nu}_e$ survival probability [Eq. (1)]. In order to properly account for the systematic effects and correlations among energy bins, a χ^2 is constructed using nuisance parameters for detector response and background and a covariance matrix for reactor-related uncertainties. The absolute normalization of the $\bar{\nu}_e$ flux is a free parameter in the fit. The fit uses $\sin^2 2\theta_{12} = 0.857 \pm 0.024$ and $\Delta m^2_{21} = (7.50 \pm 0.20) \times 10^{-5}$ eV^2 [1]. The best-fit values are $\sin^2 2\theta_{13} = 0.090^{+0.008}_{-0.009}$ and $|\Delta m^2_{ee}| = (2.59^{+0.19}_{-0.20}) \times 10^{-3}$ eV^2 with $\chi^2/\mathrm{NDF} = 163/153$ [68.3% confidence level (C.L.) intervals] (see the Supplemental Material [27]). The prompt energy spectra observed in each of the experimental halls are compared to the spectra expected for no oscillation and with the best-fit oscillation parameters in Fig. 2. The 68.3%, 95.5%, and 99.7% C.L. allowed regions in the $|\Delta m^2_{ee}|$ vs $\sin^2 2\theta_{13}$ plane are shown in Fig. 3. Under the assumption of the normal (inverted) neutrino mass hierarchy [1], this result is equivalent to $|\Delta m^2_{32}| = (2.54^{+0.19}_{-0.20}) \times 10^{-3}$ eV^2 ($|\Delta m^2_{32}| = (2.64^{+0.19}_{-0.20}) \times 10^{-3}$ eV^2). The result is consistent with $|\Delta m^2_{\mu\mu}| = (2.41^{+0.09}_{-0.10}) \times 10^{-3}$ eV^2 as measured via ν_μ and $\bar{\nu}_\mu$ disappearance [28] noting the small $\mathcal{O}(0.04 \times 10^{-3}$ eV$^2)$ effects due to other neutrino oscillation parameters. Figure 4 compares the IBD data from all experimental halls with the $\bar{\nu}_e$ survival probability [Eq. (1)] using the best-fit values. Almost one full oscillation cycle is visible, demonstrating both the amplitude and frequency of short-baseline reactor $\bar{\nu}_e$ oscillation.

The total uncertainty on both oscillation parameters is dominated by statistics. The most significant contributions to the $\sin^2 2\theta_{13}$ systematic uncertainty are the reactor, relative-detector-efficiency, and energy-scale components [29]. The $|\Delta m^2_{ee}|$ systematic uncertainty is dominated by the relative energy scale and efficiency. Consistent results

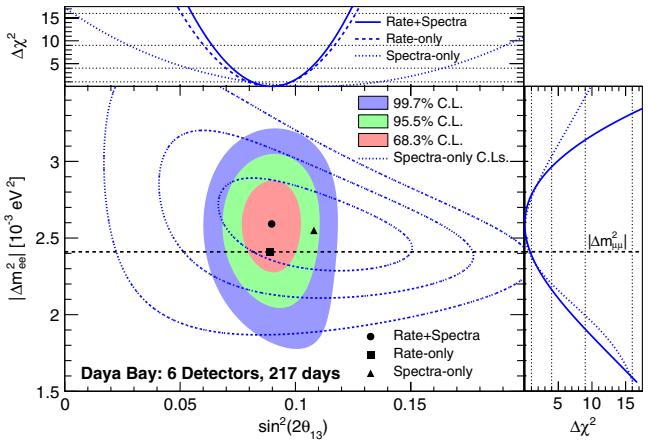

FIG. 3 (color online). Allowed regions for the neutrino oscillation parameters $\sin^2 2\theta_{13}$ and $|\Delta m^2_{ee}|$ at the 68.3%, 95.5%, and 99.7% confidence level, obtained from comparison of the rates and prompt energy spectra measured by the 3 near-site and 3 far-site antineutrino detectors (solid regions). The best estimate of the oscillation parameters is given by the black dot. The three dotted contours indicate the allowed 68.3%, 95.5%, and 99.7% C.L. regions for the spectra-only fit with the black triangle representing the best estimate of the oscillation parameters. The adjoining panels show the dependence of $\Delta\chi^2$ on $|\Delta m^2_{ee}|$ (right) and $\sin^2 2\theta_{13}$ (top). The black square and dashed curve represent the rate-only result. The dotted curves represent the spectra-only $\Delta\chi^2$ distributions. The dashed horizontal line represents the MINOS $|\Delta m^2_{\mu\mu}|$ measurement [28].

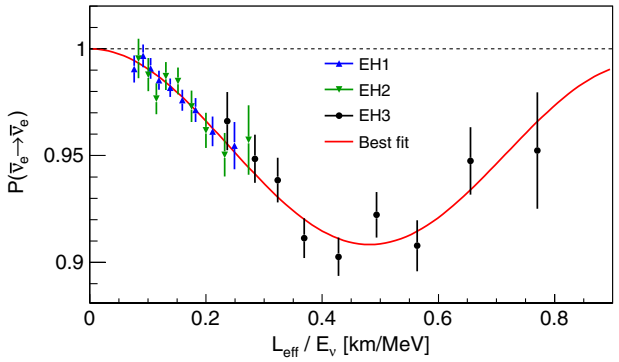

FIG. 4 (color online). Prompt positron energy spectra in the three experimental halls, reexpressed as the electron antineutrino survival probability versus propagation distance L over antineutrino energy E_ν. An effective detector-reactor distance L_{eff} is determined for each experimental hall equating the multicore oscillated flux to an effective oscillated flux from a single baseline. The best estimate of the detector response is used to convert the background-subtracted positron energy spectrum into the antineutrino energy spectrum E_ν. The horizontal location of each data point is given by the average of the counts in each bin ($\langle L_{\text{eff}}/E_\nu \rangle$). The vertical position is determined by the ratio of the counts in each bin relative to the counts expected assuming no oscillation, corrected for the reduction of analyzing power (energy dependent) due to multiple baselines and the binning in L/E. Error bars represent the statistical uncertainty only. The oscillation survival probability using the best estimates of $\sin^2 2\theta_{13}$ and $|\Delta m^2_{ee}|$ is displayed for reference.

are obtained with an independent approach that uses minimal reactor model assumptions and directly predicts the far spectra from the near spectra. Similarly, analysis with a purely nuisance-parameter-based χ^2 or purely covariance-matrix-based χ^2 yields consistent results. The rate-only result is $\sin^2 2\theta_{13} = 0.089 \pm 0.009$ with $\chi^2/\text{NDF} = 0.5/4$ with $|\Delta m^2_{ee}|$ constrained by the measurement of $|\Delta m^2_{\mu\mu}|$ [28]. The spectra-only result, obtained by fixing the predicted event rate in each AD to the measured rate, is $\sin^2 2\theta_{13} = 0.108 \pm 0.028$ and $|\Delta m^2_{ee}| = (2.55^{+0.21}_{-0.18}) \times 10^{-3}$ eV^2 with $\chi^2/\text{NDF} = 161/148$, and rules out $\sin^2 2\theta_{13} = 0$ at > 3 standard deviations.

In summary, the relative deficit and spectral distortion observed between three far and three near antineutrino detectors at Daya Bay provides the first independent measurement of $|\Delta m^2_{ee}| = (2.59^{+0.19}_{-0.20}) \times 10^{-3}$ eV^2 and the most precise estimate of $\sin^2 2\theta_{13} = 0.090^{+0.008}_{-0.009}$ to date. Following a special calibration campaign in summer 2012, data collection using all eight antineutrino detectors began in October 2012, and an eventual reduction to a few percent uncertainty in both oscillation parameters is anticipated. On-going analysis of the special calibration data is expected to yield improvements in the energy response model and the knowledge of the absolute $\bar{\nu}_e$ detection efficiency. These improvements will enable a future high-statistics measurement of the absolute reactor $\bar{\nu}_e$ flux and energy spectra that will provide a valuable reference for studies of reactor neutrinos.

The Daya Bay Experiment is supported in part by the Ministry of Science and Technology of China, the United States Department of Energy, the Chinese Academy of Sciences, the National Natural Science Foundation of China, the Guangdong provincial government, the Shenzhen municipal government, the China Guangdong Nuclear Power Group, Shanghai Laboratory for Particle Physics and Cosmology, the Research Grants Council of the Hong Kong Special Administrative Region of China, University Development Fund of The University of Hong Kong, the MOE program for Research of Excellence at National Taiwan University, National Chiao-Tung University, and NSC fund support from Taiwan, the U.S. National Science Foundation, the Alfred P. Sloan Foundation, the Ministry of Education, Youth and Sports of the Czech Republic, Charles University in Prague, Yale University, the Joint Institute of Nuclear Research in Dubna, Russia, and the NSFC-RFBR joint research program. We acknowledge Yellow River Engineering Consulting Co., Ltd., and China Railway 15th Bureau Group Co., Ltd., for building the underground laboratory. We are grateful for the ongoing cooperation from the China Guangdong Nuclear Power Group and China Light & Power Company.

[1] J. Beringer *et al.* (Particle Data Group), Phys. Rev. D **86**, 010001 (2012), Sec. 13.
[2] F. P. An *et al.* (Daya Bay Collaboration), Phys. Rev. Lett. **108**, 171803 (2012).
[3] F. P. An *et al.* (Daya Bay Collaboration), Chin. Phys. C **37**, 011001 (2013).
[4] J. Ahn *et al.* (RENO Collaboration), Phys. Rev. Lett. **108**, 191802 (2012).
[5] Y. Abe *et al.* (Double Chooz Collaboration), Phys. Rev. Lett. **108**, 131801 (2012).
[6] P. Adamson *et al.* (MINOS Collaboration), Phys. Rev. Lett. **110**, 171801 (2013).
[7] K. Abe *et al.* (T2K Collaboration), Phys. Rev. D **88**, 032002 (2013).
[8] M. Bishai, M. V. Diwan, S. Kettell, J. Stewart, B. Viren, E. Worchester, and L. Whitehead, arXiv:1203.4090.
[9] Y. F. Li, J. Cao, Y. F. Wang, and L. Zhan, Phys. Rev. D **88**, 013008 (2013).
[10] A. Balantekin *et al.*, arXiv:1307.7419.
[11] Our Δm^2_{ee} definition is consistent with H. Minakata, H. Nunokawa, S. J. Parke, and R. Zukanovich Funchal, Phys. Rev. D **74**, 053008 (2006).
[12] P. Adamson *et al.* (MINOS Collaboration), Phys. Rev. Lett. **106**, 181801 (2011).
[13] F. P. An *et al.* (Daya Bay Collaboration), Nucl. Instrum. Methods Phys. Res., Sect. A **685**, 78 (2012).
[14] F. P. An *et al.* (Daya Bay Collaboration), arXiv:hep-ex/0701029.

[15] S. Agostinelli *et al.*, Nucl. Instrum. Methods Phys. Res., Sect. A **506**, 250 (2003).
[16] J. Allison *et al.*, IEEE Trans. Nucl. Sci. **53**, 270 (2006).
[17] J. B. Birks, Phys. Rev. **84**, 364 (1951).
[18] L. J. Wen, J. Cao, K. B. Luk, Y. Q. Ma, Y. F. Wang, and C. G. Yang, Nucl. Instrum. Methods Phys. Res., Sect. A **564**, 471 (2006).
[19] G. Nyman, R. E. Azuma, P. G. Hansen, B. Jonson, P. O. Larsson, S. Mattsson, A. Richter, K. Riisager, O. Tengblad, and K. Wilhelmsen, Nucl. Phys. **A510**, 189 (1990).
[20] T. Bjornstad, H. Å. Gustafsson, B. Jonson, P. O. Larsson, V. Lindfors, S. Mattsson, G. Nyman, A. M. Poskanzer, H. L. Ravn, and D. Schardt (ISOLDE Collaboration), Nucl. Phys. **A366**, 461 (1981).
[21] K. Schreckenbach, G. Colvin, W. Gelletly, and F. von Feilitzsch, Phys. Lett. **160B**, 325 (1985).
[22] A. A. Hahn, K. Schreckenbach, W. Gelletly, F. von Feilitzsch, G. Colvin, and B. Krusche, Phys. Lett. B **218**, 365 (1989).
[23] F. von Feilitzsch, A. Hahn, and K. Schreckenbach, Phys. Lett. **118B**, 162 (1982).
[24] P. Vogel, G. K. Schenter, F. M. Mann, and R. E. Schenter, Phys. Rev. C **24**, 1543 (1981).
[25] P. Huber, Phys. Rev. C **84**, 024617 (2011).
[26] T. Mueller *et al.*, Phys. Rev. C **83**, 054615 (2011).
[27] See Supplemental Material at http://link.aps.org/supplemental/10.1103/PhysRevLett.112.061801 for a table of $\chi^2 - \chi^2_{\text{min}}$ as a function of ($\sin^2 2\theta_{13}$, $|\Delta m^2_{ee}|$).
[28] P. Adamson *et al.* (MINOS Collaboration), Phys. Rev. Lett. **110**, 251801 (2013).
[29] Define the contribution of the ith component to the total uncertainty (σ_{tot}) as $\sigma_i^2/\sigma_{\text{tot}}^2$. The contributions to the $\sin^2 2\theta_{13}$ ($|\Delta m^2_{ee}|$) uncertainty are then 0.73 (0.65), 0.18 (0.02), 0.13 (0.21), 0.11 (0.01), and 0.04 (0.06) for the statistical, reactor, relative-energy and efficiency, absolute-energy, and background components, respectively. Note that $\sum_i \sigma_i^2/\sigma_{\text{tot}}^2 \neq 1$ due to correlations.